Phase Diagram of Syndiotactic Polypropylene: Influence of Stereoregularity and Temperature on the Polymorphic Behavior

Odda Ruiz de Ballesteros,* Finizia Auriemma, and Claudio De Rosa

Dipartimento di Chimica, Università di Napoli "Federico II", Complesso Monte S. Angelo, Via Cintia 80126, Napoli, Italy

Received August 2, 2006; Revised Manuscript Received November 6, 2006

ABSTRACT: A method for building the phase diagram of syndiotactic polypropylene in stretched fibers as a function of stereoregularity, degree of deformation, and temperature is reported. The method is based on the analysis of the X-ray fiber diffraction patterns of samples of different stereoregularity, prepared with different metallocene catalysts and stretched at different degrees of deformation and stretching temperatures. For all the analyzed samples the boundary lines between the different regions of stability of the different polymorphic forms have been determined by the emergence or disappearance of X-ray reflections typical of the different forms. Although the phase diagram is given from a dynamic rather than a thermodynamic perspective, the polymorphic forms observed by X-ray diffraction correspond to the equilibrium modifications, thermodynamically stable at those values of stereoregularity and deformation.

Introduction

Syndiotactic polypropylene (s-PP) has recently received large interest thanks to its remarkable physical and mechanical properties.[1−6] In fact, depending on the stereoregularity and morphology s-PP samples exhibit variable mechanical behavior, from stiff plastic to flexible elastomeric materials. Unoriented films of highly stereoregular s-PP samples, with concentration of *rrrr* pentad higher than 75%, indeed behave as rigid thermoplastic material undergoing irreversible deformation upon stretching and small elastic recovery. Oriented fibers of highly stereoregular samples, instead, show good elastic properties with nearly total recovery of the dimension of the specimens upon successive stretching and relaxation cycles.[1,3,5] The mechanical properties drastically change in low stereoregular s-PP samples, with concentration of *rrrr* pentad in the range 45−70%.[6] In fact, contrary to highly stereoregular and crystalline s-PP, low syndiotactic samples present good elastic properties even for unoriented films and behave like typical thermoplastic elastomers.[6b]

The variability in the physical and mechanical properties of s-PP is related to the complex polymorphism in the solid state due to the presence of four different crystalline forms[7−18] and a mesomorphic form.[19−21] The various crystalline forms are characterized by chains in helical (forms I and II)[7,9−15] and trans-planar conformations (form III and mesomorphic form)[8,10,13,16,19−21] and transform each other in different crystallization and processing conditions, as, for instance, by annealing,[10,13,22] stretching,[3,5,10,13] or relaxation of stretched fibers by removing the tension.[3,5,13]

This complex picture is further complicated by the fact that the crystallization behavior and the polymorphic transformations, and, in turn, the physical and mechanical properties, depend on the microstructure of the polymer chain, in particular on the stereoregularity.[3a,6,12,21]

It has been extensively reported that the plastic deformation of s-PP samples is generally associated with polymorphic transformations.[3−6,10,13,23] The crystalline form present in melt-crystallized samples in spherulitic morphology (generally the helical form I) transforms by stretching into crystalline forms with chains in the trans-planar conformation with fibrillar morphology.[10,13] Furthermore, it has also been shown that during plastic deformation of crystalline polymers the position of the critical strain at which a critical network stress is achieved, which produces breaking of crystal blocks and recrystallization with formation of fibrils, depends on the interplay between the modulus of the entangled amorphous and the intrinsic stability of crystals.[23,24] Preliminary data have indicated that in the case of s-PP the critical values of strain at which the polymorphic transformation starts and at which the transition is complete depend on the stereoregularity.[25] The stability of crystals of the different polymorphic forms of s-PP involved in the transformations during plastic deformation and the entanglement density of amorphous chains depend, indeed, on the stereoregularity.[25]

Since the transformation of the stable helical form I of s-PP into the trans-planar forms occurs by dynamic experiments as tensile deformation, the condition of stability of the various polymorphic forms may also depend on nonthermodynamic parameters such as the deformation rate. For this reason the definition of a thermodynamic phase diagram of s-PP where the region of stability of the various polymorphic forms of s-PP as a function of stereoregularity, degree of deformation, and temperature is not a simple task.

In this paper we report a method for building the phase diagram of s-PP, based on the analysis of the X-ray fiber diffraction patterns of samples of different stereoregularity stretched at different degrees of deformation and stretching temperatures. With this method the polymorphic forms observed by X-ray diffraction correspond to the equilibrium modifications, thermodynamically stable at those values of stereoregularity and deformation, and the phase diagram gives the regions of stability of the helical and trans-planar forms of s-PP as a function of strain, stereoregularity, and temperature.

Experimental Section

Seven different samples of s-PP having different stereoregularity have been prepared with different metallocene catalysts shown in Chart 1. The properties of the analyzed samples are listed in Table 1.

* Corresponding author: Tel ++39 081 674448; Fax ++39 081 674090; e-mail odda.ruizdeballesteros@unina.it.

10.1021/ma061749i CCC: $37.00
Published on Web 01/04/2007

Chart 1. Structures of Zirconocene and Titanocene Complexes Used as Catalysts for Synthesis of s-PP Samples of Different Stereoregularity

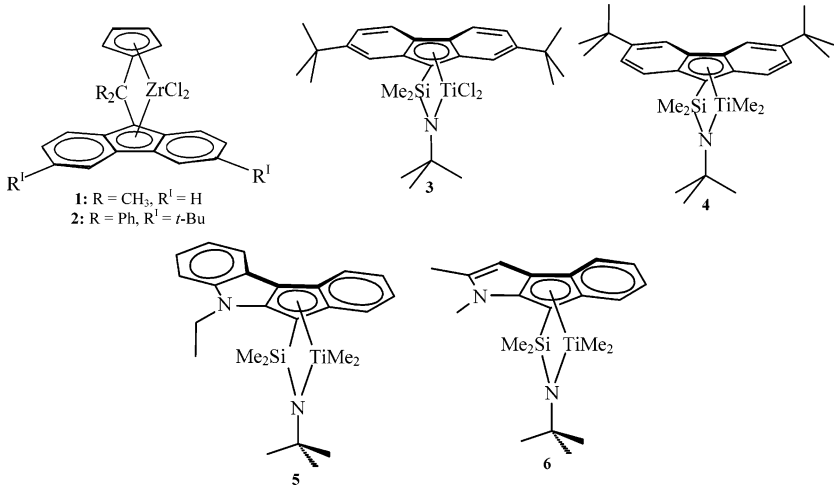

Table 1. Polymerization Temperatures (T_p), Molecular Masses (M_w), Concentration of Fully Syndiotactic Pentad ([*rrrr*]), Melting Temperatures (T_m), and Degrees of Crystallinity (x_c) of s-PP Samples Prepared with Catalysts 1−6 of Chart 1

sample	T_p (°C)	catalyst	M_w[a]	[*rrrr*] (%)	T_m (°C)[b]	x_c (%)
sPP1	40	**2**	766 000	91.5	150	48
sPP2	60	**2**	509 000	87.0	121−142[c]	43
sPP3	40	**1**	193 000	78.0	124	35
sPP4	80	**3**	297 000	70.6	100	31
sPP5	80	**4**	241 000	60.1	77	28
sPP6	70	**5**	1 308 600	54.6	59	20
sPP7	80	**6**	1 153 200	45.8	48	16

[a] From GPC. [b] Measured from DSC scans at heating rate of 10 °C/min. [c] The two values correspond to the two endothermic peaks present in the DSC curve due to recrystallization phenomena.

Sample sPP3 was prepared with the classic syndiospecific C_s-symmetric catalyst **1** of Chart 1, isopropylidene(cyclopentadienyl)-(9-fluorenyl)zirconium dichloride ($Me_2C(Cp)(9\text{-}Flu)ZrCl_2$, Me = methyl, Cp = cyclopentadienyl, Flu = fluorenyl), activated with methylaluminoxane (MAO).[26] Samples sPP1 and sPP2 were polymerized at different temperatures using catalyst **2** of Chart 1 ($Ph_2C(Cp)(3,6\text{-}t\text{-}Bu_2Flu)ZrCl_2$, Ph = phenyl, *t*-Bu = *tert*-butyl), in which a di-*tert*-butyl-substituted fluorenyl ligand is present.[27] Samples sPP4 and sPP5 were prepared with the "constrained geometry" catalysts **3** and **4** of Chart 1, respectively, composed of fluorenylsilylamido complexes of titanium, [$Me_2Si(2,7\text{-}t\text{-}Bu_2Flu)$-($t$-BuN)]$TiCl_2$[28] (**3** of Chart 1) and [$Me_2Si(3,6\text{-}t\text{-}Bu_2Flu)(t\text{-}BuN)$]-$TiCl_2$[29] (**4** of Chart 1). Finally, samples sPP6 and sPP7 were prepared with constrained geometry catalysts **5** and **6** of Chart 1, respectively, composed of indenylsilylamido complexes of Ti in which the indenyl ligand has a heterocycle condensed onto the Cp moiety.[6a,30] These Ti complexes are highly active and produce s-PP samples of high molecular masses with concentration of the fully syndiotactic pentad *rrrr* in the range 45−70% (see Table 1).[28−30]

Samples sPP1−sPP5 were provided by Dr. Abbas Razavi of ATOFINA Research (Feluy, Belgium), whereas samples sPP6 and sPP7 were provided by Dr. Luigi Resconi of Basell Polyolefins (Ferrara, Italy).

Unoriented films with thickness of 0.3−0.5 mm were prepared by compression-molding of as-polymerized samples. Powders of s-PP samples have been heated at temperatures 30−40 °C higher than the melting temperatures of the as-prepared samples and slowly cooled to room temperature. For highly stereoregular samples, with concentration of *rrrr* pentad higher than 70% (samples sPP1−sPP3), this procedure generally produces crystalline films in the helical form I, whereas for less stereoregular samples (samples sPP4−sPP7), amorphous specimens are obtained. Crystallization of these amorphous samples has been performed keeping the compression-molded specimens at room temperature for several days. The samples slowly crystallize in disordered modifications of the helical form I of s-PP, and a maximum crystallinity is achieved after 1 week of aging at room temperature.[6a] The degrees of crystallinity of the compression molded films of s-PP decreases with decreasing stereoregularity (see Table 1).

Oriented fibers have been obtained by stretching crystalline compression-molded films at different temperatures of 6, 25, 60, and 80 °C and at different deformations ϵ ($\epsilon = 100(L_f - L_i)/L_i$, with L_i and L_f the initial and final lengths of the specimen, respectively). Two benchmarks have been placed on the test specimens and used to measure elongation.

X-ray diffraction patterns were obtained with Ni-filtered Cu Kα radiation. The powder profiles were obtained with an automatic Philips diffractometer, whereas the fiber diffraction patterns were recorded on a BAS-MS imaging plate (FUJIFILM) using a cylindrical camera (radius 57.3 mm) and processed with a digital imaging reader (FUJIBAS 1800). The diffraction patterns have been recorded at room temperature for stretched fibers soon after the stretching, while keeping the fiber under tension. During deformation the focused X-ray beam always illuminates the same position of the film between the two benchmarks. Therefore, the measured strain basically corresponds to the true strain. The exposure time is at least 2 h; therefore, each fiber is kept in tension at the given deformation and temperature for 2 h. This time is long enough and ensures full relaxation of the sample so that the crystalline form observed by X-ray at that deformation and temperature probably corresponds to the equilibrium form, thermodynamically stable for those values of deformation and temperature.

The degrees of crystallinity of oriented fibers have been evaluated from the X-ray fiber diffraction patterns. Monodimensional X-ray intensity profiles as a function of 2θ have been obtained from the bidimensional diffraction patterns by integrating the intensity along the azimuthal angle with constant value of 2θ, at interval of $\Delta 2\theta = 0.4°$, in the 2θ range 10°−30°. The diffraction profile of the amorphous phase has been evaluated performing the same procedure, from the bidimensional X-ray diffraction pattern of a sample of atactic polypropylene, obtained with the same cylindrical camera. The amorphous profile was then scaled and subtracted from the X-ray diffraction profiles of the crystalline fibers. The degree of crystallinity was therefore calculated from the ratio of the so-obtained crystalline diffracting area and the total area of the original X-ray diffraction profile.

At each value of deformation, the fibers are composed of mixtures of the helical form I, the trans-planar form III, and/or the trans-planar mesomorphic form, whose concentrations depend on the stereoregularity. The amount of crystals of helical and trans-planar forms present in the fibers stretched at different temperatures and deformations was evaluated by the diffraction profiles read along the equator of the X-ray fiber diffraction patterns. In

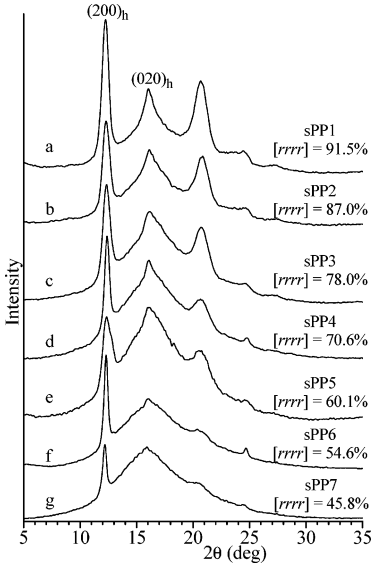

Figure 1. X-ray powder diffraction profiles of compression-molded films of s-PP samples of different stereoregularity. The samples sPP4−sPP7 are amorphous after the compression-molding and have been crystallized by aging at room temperature. The $(200)_h$ and $(020)_h$ reflections at $2\theta = 12°$ and 16°, respectively, of the helical form I are indicated.

particular, the fraction of crystals of polymorphic forms with chains in trans-planar conformation ($f_{trans-planar}$), i.e., the crystalline form III, the mesomorphic form, or a mixture of both, was determined by subtracting from the whole equatorial fiber diffraction profile the amorphous contribution and the equatorial profile of the crystalline helical form I, scaled for a suitable factor. The amorphous halo along the equatorial line was obtained from the equatorial diffraction profile of the bidimensional X-ray diffraction pattern of atactic polypropylene, whereas the contribution of the helical form I was obtained from the equatorial diffraction profile of the bidimensional X-ray diffraction pattern of a compression-molded film of the same s-PP sample in the pure helical form I. The estimated error in the determination of the fraction of crystals of trans-planar forms ($f_{trans-planar}$) is about 3%.

Results and Discussion

The X-ray powder diffraction profiles of compression-molded films of s-PP samples of Table 1 are reported in Figure 1. Less stereoregular samples sPP4−sPP7, with *rrrr* pentad content lower than 70%, do not crystallize by cooling from the melt to room temperature. However, the amorphous samples slowly crystallize by aging at room temperature for about 1 week. The diffraction profiles d−g of Figure 1 correspond to samples aged at room temperature to achieve the maximum crystallinity. All samples crystallize in disordered modifications of the helical form I, as indicated by the presence in the diffraction profiles of Figure 1 of the $(200)_h$ and $(020)_h$ reflections at $2\theta = 12°$ and 16°, respectively, and the absence of the $(211)_h$ reflection at $2\theta = 18.8°$. The degree of crystallinity, evaluated from the X-ray diffraction profiles of Figure 1 and reported in Table 1, decreases with decreasing stereoregularity.

In our previous paper we analyzed the polymorphic behavior of s-PP under tensile deformation at room temperature and found that the stress-induced phase transitions are strain-controlled rather than stress-controlled.[25] We have shown that the values of critical strain at which the well-known polymorphic transition of the helical form I into the trans-planar form III starts, and at which the transition is complete, depend on the stereoregularity.[25] This can be easily explained considering that the position of the critical strain at which a critical network stress is achieved, which produces breaking of crystal blocks and recrystallization with formation of fibrils, depends on the interplay between the modulus of entangled amorphous and the intrinsic stability of crystals.[23,24] Therefore, when a polymorphic transition occurs along with the morphological plastic transformation, the relative stability of the polymorphic forms involved in the transformations and the state of the entangled amorphous phase are affected by the stereoregularity of the polymer samples.[25]

In particular, we have reported that during stretching of highly stereoregular s-PP sample, with [*rrrr*] > 90%, when a critical value of the strain $\epsilon_c = 90-100\%$ is achieved, the stable helical form I initially present in the unoriented film (Figure 1) transforms into the trans-planar form III.[25] The value of the critical strain ϵ_c increases with decreasing stereoregularity. These data allowed us building the phase diagram of s-PP at room temperature where the regions of stability of the different polymorphic forms of s-PP in oriented fibers are defined as a function of degree of stereoregularity and deformation.[25] In this paper we present similar data obtained by stretching samples of different stereoregularity at different temperatures aimed at building a complete phase diagram of s-PP as a function of stereoregularity, degree of deformation, and temperature. However, since some transient phenomena occur during deformation at low values of strain at room temperature, some data at room temperature are represented here and compared with the data at different temperatures.

The X-ray fiber diffraction patterns of samples sPP1 and sPP3 stretched at room temperature and at different deformations are reported in Figure 2. The corresponding diffraction profiles read along the equatorial line are reported in Figure 3. For the most stereoregular sample sPP1, the helical form I starts transforming into the trans-planar form III at the critical strain $\epsilon_c = 90-100\%$ (Figures 2B and 3A). The transformation is complete at a minimum value of the strain ϵ_m of nearly 300%.

For the less stereoregular sample sPP3, with [*rrrr*] = 78%, when the critical strain is achieved, the helical form I starts transforming into the mesomorphic form rather than into the trans-planar form III (Figures 2F,G and 3B). The mesomorphic form then transforms into the trans-planar form III at higher deformations, and only at $\epsilon_m = 600\%$ (Figures 2H and 3B) is the pure form III obtained.

Finally, for low syndiotactic and poorly crystalline s-PP samples, with [*rrrr*] = 45−70%, the crystalline trans-planar form III does not form by stretching, even at very high deformations. The disordered helical form I, initially present in the unoriented films (Figure 1), gradually transforms by stretching into the disordered trans-planar mesomorphic form.[6c]

The degree of crystallinity of the s-PP samples does not change significantly during stretching and remains almost equal to that of the initial unoriented compression-molded film. In particular, values of crystallinity around 40−60% have been evaluated for highly stereoregular samples, with syndiotactic *rrrr* pentad concentration in the range 78−92%, and around 16−20% for less stereoregular samples, with [*rrrr*] in the range 46−70%. This indicates that the transformation of form I into form III for more stereoregular samples (with [*rrrr*] > 90%), and into the mesomorphic form for samples of lower stereoregularity (with [*rrrr*] < 90%), is probably originated by mechanical melting of form I lamellae, with consequent formation of a disentangled amorphous, followed by fast recrystallization into the trans-planar form III or mesomorphic form, and only marginally by crystallization of the amorphous phase during stretching.

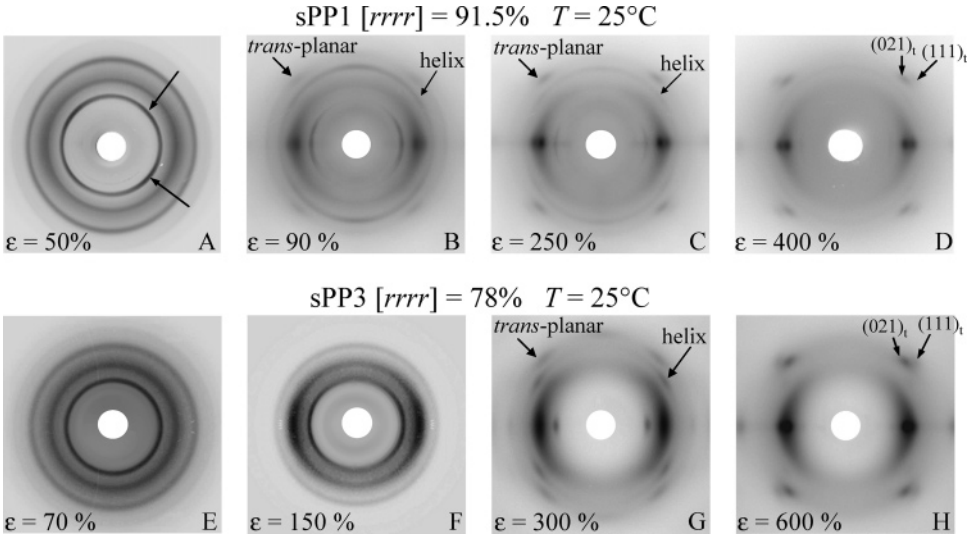

Figure 2. X-ray fiber diffraction patterns of fibers of the samples sPP1 with [*rrrr*] = 91.5% (A−D) and sPP3 with [*rrrr*] = 78% (E−H), stretched at room temperature at the indicated values of deformation ϵ. On the first layer line reflections corresponding to helical and trans-planar conformations ($(021)_t$ and $(111)_t$ reflections in the case of the crystalline form III) are indicated. The arrows in (A) evidence the polarization of the $(200)_h$ reflection at oblique angles due to orientation of a portion of the crystalline lamellae with the chain axes nearly perpendicular to the stretching direction.

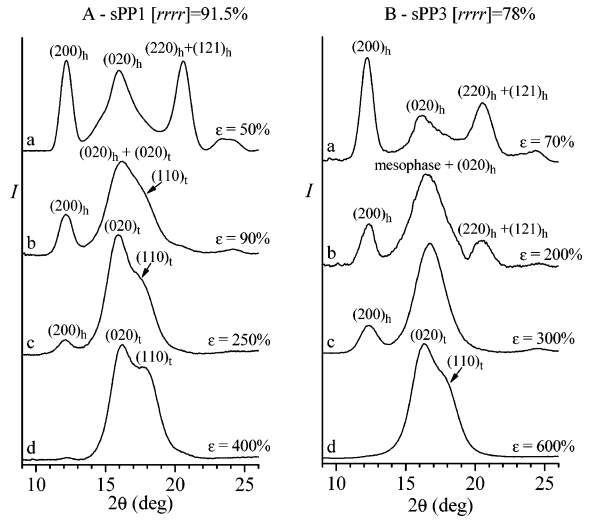

Figure 3. X-ray diffraction profiles read along the equatorial line, after the subtraction of the amorphous contribution, of the X-ray diffraction patterns of fibers of the samples sPP1 with [*rrrr*] = 91.5% (A) and sPP3 with [*rrrr*] = 78% (B), stretched at 25 °C at the indicated values of deformation ϵ. The $(200)_h$, $(020)_h$, $(220)_h$, and $(121)_h$ reflections of the helical form I and the $(020)_t$ and $(110)_t$ reflections of the trans-planar form III are indicated.

It is worth noting that for deformations below the critical value, before the development of the fibrillar morphology, transient changes of the sample texture also occur, consisting in the orientation of portion of the crystalline lamellae with the chain axes nearly perpendicular to the stretching direction instead than parallel as in the standard fiber morphology. This nonstandard crystals orientation is achieved, for instance, in the case of the more stereoregular sample sPP1 at $\epsilon = 50\%$ (Figure 2A), as indicated by the polarization of the $(200)_h$ reflection at $2\theta = 12°$ at oblique angles (arrowed in Figure 2A). At higher deformations, the diffraction maxima at oblique angles disappear, and the $(200)_h$ reflection is polarized on the equator, as in the standard fiber morphology (Figure 2B). As argued in refs 23 and 24, this change in the texture at low deformations is induced by interlamellar and intralamellar slip processes. Interlamellar shear leads to a location of the $(200)_h$ reflections on the meridian, corresponding to the chain axes perpendicular to the stretching direction, while the intralamellar shear pushes the chain axes to align parallel with the stretching direction and thus shifts the position of the $(200)_h$ reflection toward the equator. This mechanism is widely general[23,24,31,32] and reflects crystallographic restraints on the slip processes during deformation. The $(200)_h$ planes of form I of s-PP, indeed, correspond to the planes of maximum packing of the 2-fold helices.[9d]

At each value of deformation, the fibers are composed of mixtures of crystals of the helical form I, the trans-planar form III, and/or the trans-planar mesomorphic form. Therefore, the X-ray diffraction patterns of the kind of Figures 2 and 3 at intermediate deformations are the sum of two or three components, depending on the stereoregularity. The fraction of crystals of polymorphic forms with chains in trans-planar conformation ($f_{trans-planar}$), that is, the crystalline form III, the mesomorphic form, or a mixture of both, was determined from the whole equatorial diffraction profiles of Figure 3 by subtracting the contribution of the amorphous phase and of the helical form I. Since it is not possible to obtain oriented s-PP fibers in pure helical form I, because form I transforms into the trans-planar forms by stretching, the contribution of crystals of the helical form I to the whole equatorial diffraction profile has been evaluated at any value of the strain from a simulated equatorial profile of the pure helical form I, suitably scaled. For each sample of a given stereoregularity the simulated equatorial profile of form I has been obtained, in turn, from the diffraction profile read along the equatorial line of the bidimensional X-ray diffraction pattern of unoriented compression-molded films crystallized in form I, by the fitting with Gaussian components corresponding to all reflections of form I. This procedure is shown as an example in Figure 4 for the sample sPP1 stretched at room temperature at 90% strain.

The diffraction profiles read along the equatorial line of the bidimensional X-ray diffraction patterns of an unoriented film of the sample sPP1 in the pure helical form I and of a fiber of the same sample stretched at 90% strain (Figure 2B) are shown in parts A and B of Figure 4, respectively. The diffraction profile of the amorphous phase, obtained by the diffraction profile read along the equatorial line of the bidimensional X-ray diffraction pattern of atactic polypropylene, is also reported in Figure 4 (dashed lines) after scaling by a suitable factor. The diffraction profiles of the unoriented sample sPP1 (Figure 4A) and that of

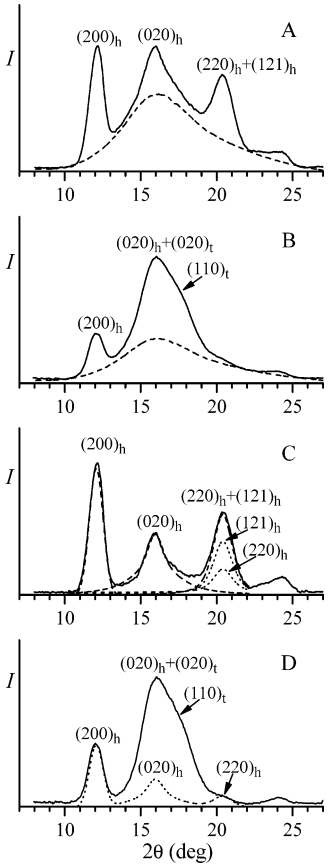

Figure 4. (A) X-ray diffraction profile read along the equatorial line of the bidimensional X-ray diffraction pattern of the compression-molded film of the sample sPP1, having [*rrrr*] = 91.5%, crystallized in the helical form I. (B) X-ray equatorial profile of the diffraction pattern of fibers of the sample sPP1 stretched at 90% strain of Figure 2B. The amorphous components, obtained by the equatorial diffraction profile of the bidimensional X-ray diffraction pattern of atactic polypropylene, after scaling by suitable factors, are indicated in (A) and (B) as dashed lines. (C) X-ray diffraction profile of the sample sPP1 in the pure helical form I (A) after the subtraction of the amorphous halo (solid line) and its four Gaussian components centered at $2\theta = 12.2°$, 15.8°, and 20.6°, corresponding to the $(200)_h$, $(020)_h$, and $(220)_h + (121)_h$ reflections of the helical form I, respectively (dashed lines). The Gaussian components corresponding to the separated $(220)_h$ and $(121)_h$ reflections of form I at $2\theta = 20.6°$ are indicated as dotted lines. (D) X-ray diffraction equatorial profile of fibers of the sample sPP1 stretched at 90% strain (B) after the subtraction of the amorphous halo (solid line) and simulated equatorial diffraction profile of the helical form I (dotted line), obtained by the sum of the Gaussian components corresponding to the equatorial $(200)_h$, $(020)_h$, and $(220)_h$ reflections reported in (C), scaled by a suitable factor so that the intensities of the $(200)_h$ reflection at $2\theta = 12°$ in the simulated diffraction profile of the helical form I and in the experimental profile of the fiber stretched at 90% deformation are equal. In all parts A−D the $(200)_h$, $(020)_h$, and $(220)_h + (121)_h$ reflections of the helical form I at $2\theta = 12°$, 15.8°, and 20.6°, respectively, and the $(020)_t$ and $(110)_t$ reflections of the trans-planar form III at $2\theta = 16°$ and 18.2°, respectively, are also indicated.

the fiber of the same sample stretched at 90% deformation (Figure 4B), after the subtraction of the amorphous halo, are shown in Figure 4C,D (solid line).

The diffraction profile of the unoriented sample sPP1 in the pure helical form I (Figure 4C) does not correspond to the equatorial profile of the helical form I, as it includes also the contribution of the first layer line $(121)_h$ reflection. In fact, this profile can be separated into four Gaussian components centered at $2\theta = 12.1°$, 16.0°, and 20.4°, corresponding to the $(200)_h$, $(020)_h$, and $(220)_h + (121)_h$ reflections of the helical form I, respectively, shown in Figure 4C (dashed lines). The peak at

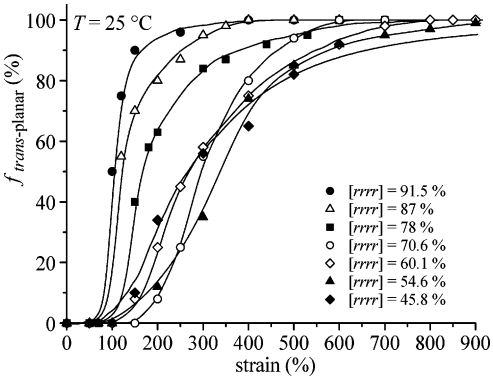

Figure 5. Fraction of crystals of trans-planar forms ($f_{trans-planar}$), the trans-planar form III, and the mesomorphic form, present in the fibers of the samples sPP1−sPP7 stretched at room temperature as a function of strain.

$2\theta = 20.4°$ is further separated in two contributes relative to the $(220)_h$ and $(121)_h$ reflections (dotted lines in Figures 4C), assuming the ratio between the intensity of the two peaks $I(220)_h/I(121)_h$ equal to the ratio between the squares of the calculated structure factors of the two reflections $|F(220)_h|^2/|F(121)_h|^2$ of the helical form I in the space group *Ibca*, taken from ref 10. The correction by the Lorentz and polarization factor is not necessary since the 2θ diffraction angle of the two reflections is the same, and the sample is not oriented. Therefore, the sum of the Gaussian components corresponding to the only equatorial $(200)_h$, $(020)_h$, and $(220)_h$ reflections gives the equatorial diffraction profile of the helical form I, which may be taken as the contribution, after scaling, of the crystalline helical form I on the equator to the diffraction pattern of the fiber of the sample sPP1 stretched at 90% strain. This simulated equatorial profile is reported in Figure 4D (dotted line) scaled by a suitable factor so that the intensity of the $(200)_h$ reflection at $2\theta = 12°$ in the simulated diffraction profile of the helical form I coincides with that of the $(200)_h$ reflection in the profile of the fiber stretched at 90% deformation.

The fraction of crystals of polymorphic forms with chains in trans-planar conformation ($f_{trans-planar}$) in the stretched fiber is calculated from the different components in the diffraction profile of Figure 4D as

$$f_{trans-planar} = 100(A_{Tot} - A_h)/A_{Tot}$$

where A_{Tot} is the area of the equatorial diffraction profile of the fiber stretched at 90% deformation after subtraction of the amorphous contribution (solid line in Figure 4D), corresponding to the diffraction contributions on the equator of the crystalline trans-planar and helical phases, and A_h is the area of the simulated equatorial diffraction profile (dotted line in Figure 4D), corresponding to the diffraction contribution on the equator of crystals of the helical form I.

The same procedure has been used for all fibers of the samples sPP1−sPP7 stretched at different values of deformation and temperature. In particular, for the different samples sPP1−sPP7, the simulated equatorial diffraction profiles of the helical form I, which have to be subtracted from the equatorial diffraction profiles of the stretched fibers, have been obtained by the diffraction profiles read along the equatorial line of the bidimensional X-ray diffraction patterns of compression-molded films of the corresponding samples sPP1−sPP7.

The fractions of crystals in trans-planar forms ($f_{trans-planar}$), that is, the trans-planar form III and the trans-planar mesomorphic form, present in the fibers of the samples sPP1−sPP7

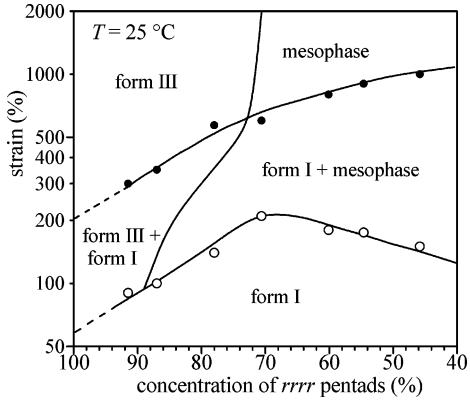

Figure 6. Phase diagram of s-PP at room temperature as a function of strain and stereoregularity.

stretched at room temperature are reported in Figure 5 as a function of the degree of deformation ϵ.

It is worth noting that, for the highly stereoregular sample sPP1 with [*rrrr*] = 91.5%, for which the helical form I initially present in the unstretched material transforms by stretching directly in the trans-planar form III, without involving the formation of a disordered intermediate phase (Figures 2A−D and 3A), the values of $f_{trans-planar}$ reported in Figure 5 correspond to the fraction of crystals of form III present in the fibers at each deformation. For the less stereoregular samples sPP2 and sPP3, with [*rrrr*] = 87 and 78%, respectively, for which the transition of the helical form I into the ordered form III involves the formation at intermediate strains of the disordered mesomorphic form (Figures 2E−H and 3B), $f_{trans-planar}$ corresponds to the sum of the fractions of crystals of form III and of the mesomorphic form. Finally, for the poorly syndiotactic samples sPP4−sPP7, for which form III does not form by stretching and the helical form I transforms directly into the mesomorphic form by stretching,[6] $f_{trans-planar}$ corresponds to the fraction of crystals of the trans-planar mesomorphic form.

The data of Figure 5 have been used to estimate the values of the critical strain ϵ_c at which the polymorphic transition of the helical form into the trans-planar forms starts and the minimum value of strain ϵ_{min} at which the transition is complete. In particular, the values of ϵ_c have been derived from the values of strain corresponding to the maximum change of the slope of the curves of Figure 5, that is, from the emergence of X-ray diffraction reflections typical of the trans-planar forms during deformation (form III or mesomorphic form). The values of ϵ_{min} have been derived from the smallest values of strain at which $f_{trans-planar} = 100\%$, that is, from the disappearance of reflections typical of the helical form I (for instance, the $(200)_h$ reflection at $2\theta = 12°$). The so-obtained values of ϵ_c and ϵ_{min} have allowed building the phase diagram of s-PP at room temperature,[25] reported in Figure 6, where the regions of stability of the different polymorphic forms of s-PP in oriented fibers are defined as a function of degree of stereoregularity and deformation.

The boundary lines between the different regions in the phase diagram of Figure 6 have been determined by using the plot of Figure 5 and also by checking the emergence or disappearance of X-ray diffraction reflections typical of the different polymorphic forms of s-PP. In particular, the phase boundary between helical form I and (form I + form III) in the more stereoregular samples, with *rrrr* concentration between 89 and 93%, has been determined using the procedure described above (from the values of ϵ_c corresponding to the maximum change of the slope of the curves of Figure 5, due to the emergence of the $(020)_t$ and $(110)_t$ reflections of the trans-planar form III at $2\theta = 16°$ and 18.2° and the decrease of the intensity of the $(200)_h$ reflection at $2\theta = 12°$ of the helical form I), and also by checking the emergence during deformation of reflections on the first layer line corresponding to the trans-planar periodicity of 5.1 Å of the trans-planar form III. The phase boundary between (form I + form III) and form III has been found from the values of ϵ_{min} at which $f_{trans-planar} = 100\%$ in Figure 5, derived from the disappearance of the typical $(200)_h$ reflection at $2\theta = 12°$ of the helical form I, and also by checking the disappearance of the $(121)_h$ reflection on the first layer line corresponding to the helical periodicity of 7.4 Å.

The phase boundary between helical form I and (form I + mesophase) in the s-PP samples with *rrrr* concentration between 45.8 and 89% has been determined from the data of Figure 5 (that is, from the values of ϵ_c corresponding to the maximum change of the slope of the curves of Figure 5, due to the emergence of the broad equatorial reflection at $2\theta = 17°$, typical of the mesomorphic form) and also by checking the emergence of the reflection on the first layer line at $2\theta \approx 24°$, corresponding to the trans-planar periodicity. Therefore, the emergence of these reflections allows distinguishing the development by stretching of the trans-planar form III, in the case of highly stereoregular samples, from that of the trans-planar mesomorphic form, in the case of less stereoregular samples.

The emergence of reflections of form III, starting from the mixture (form I + mesophase), allows finding the boundary between (form I + mesophase) and (form I + form III) for samples with *rrrr* concentration between 89 and 70%.

For samples of very low stereoregularity, with *rrrr* concentration in the range 46−70%, the ordered trans-planar form III does not form and the helical form I transforms by stretching at high deformations into the disordered mesophase. The emergence of the broad equatorial reflection at $2\theta = 17°$ and of reflections on the first layer line corresponding to the trans-planar periodicity allows determining the boundary between form I and (form I + mesophase), whereas the disappearance of reflections of the helical form at higher deformation (at values of ϵ_{min} at which $f_{trans-planar} = 100\%$ in Figure 5) and the presence of the pure mesomorphic form allow defining the boundary between (form I + mesophase) and pure mesophase. However, in the case of s-PP samples with *rrrr* concentration between 45 and 55%, the boundary between (form I + mesophase) and mesophase could not be determined from complete disappearance of $(200)_h$ and $(121)_h$ reflections of the helical form I in the X-ray fiber diffraction patterns because these samples break before the complete transformation of the helical form I into the mesomorphic form, that is, at values of deformation where the reflections of form I are still present. In these cases the values of strain at which this transition is complete, corresponding to the boundary between (form I + mesophase) and mesophase, have been determined by extrapolation of the curves of Figure 5 to $f_{trans-planar} = 100\%$.

It is worth noting that the different forms of s-PP in the phase diagram are not considered from thermodynamic standpoint but from the structure standpoint, based on the X-ray diffraction observations. Although the phase diagrams are given from a dynamic perspective rather than from a thermodynamic perspective, the used method guarantees that the critical values of strain, associated with the polymorphic transformations defining the boundary between different regions, are not affected by the deformation rate. In fact, the samples are kept in tension for 2 h during recording the X-ray fiber diffraction patterns, allowing full relaxation of the test specimen, and the observed polymor-

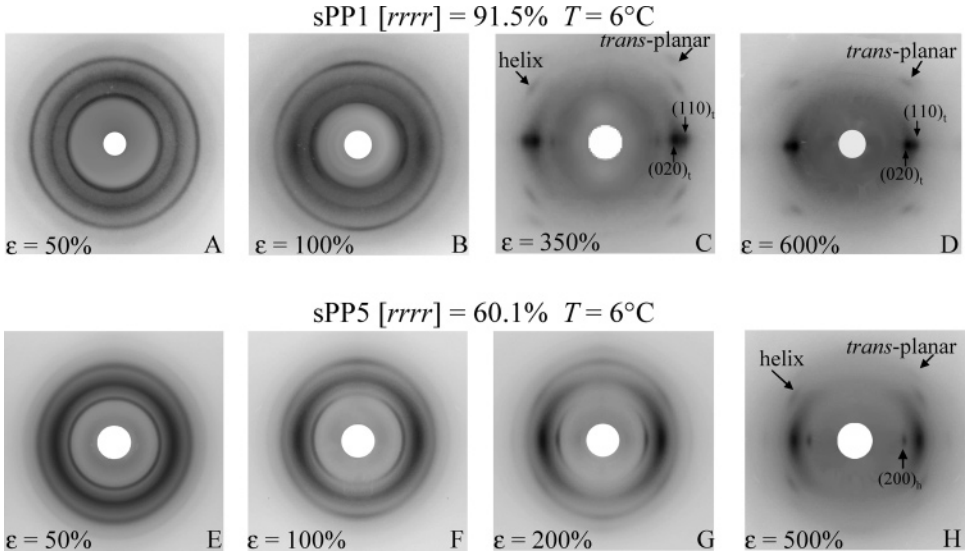

Figure 7. X-ray fiber diffraction patterns of fibers of the samples sPP1 with [*rrrr*] = 91.5% (A−D) and sPP5 with [*rrrr*] = 60.1% (E−H), stretched at 6 °C at the indicated values of deformation ϵ. The $(200)_h$ reflection of the helical form I and the $(020)_t$ and $(110)_t$ reflections of the trans-planar form III are indicated. On the first layer line reflections corresponding to helical and trans-planar conformations are indicated.

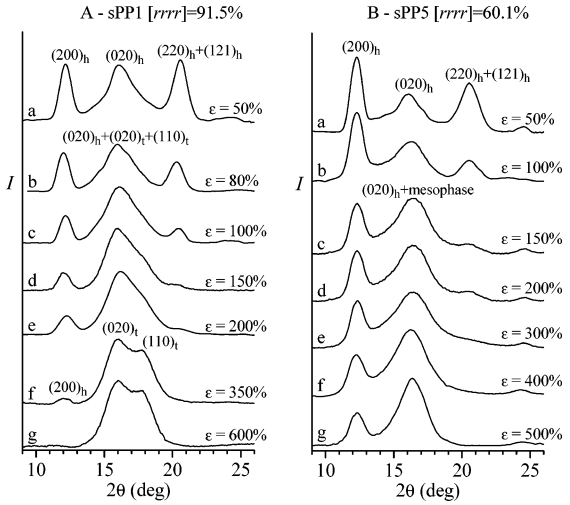

Figure 8. X-ray diffraction profiles read along the equatorial line, after the subtraction of the amorphous contribution, of the X-ray diffraction patterns of fibers of the samples sPP1 with [*rrrr*] = 91.5% (A) and sPP5 with [*rrrr*] = 60.1% (B), stretched at 6 °C at the indicated values of deformation ϵ. The $(200)_h$, $(020)_h$, $(220)_h$, and $(121)_h$ reflections of the helical form I and the $(020)_t$ and $(110)_t$ reflections of the trans-planar form III are indicated.

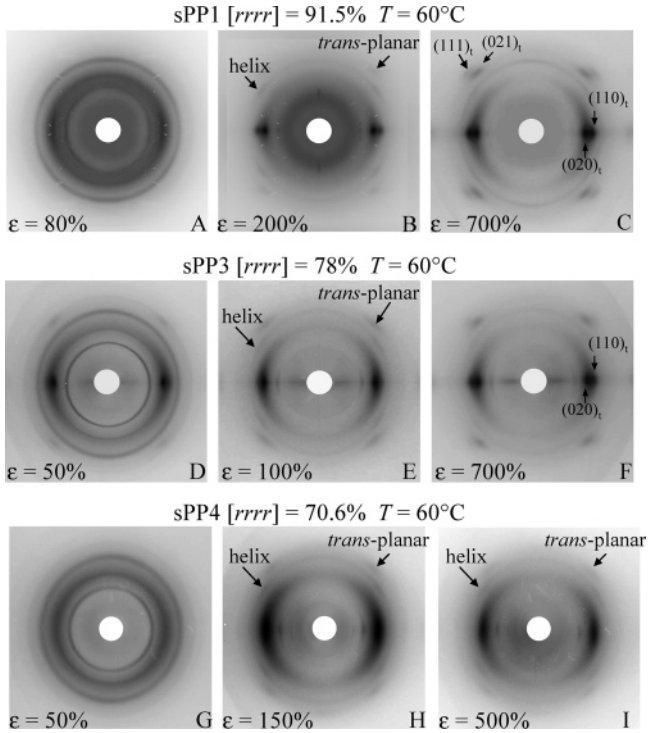

Figure 9. X-ray fiber diffraction patterns of fibers of the samples sPP1 with [*rrrr*] = 91.5% (A−C), sPP3 with [*rrrr*] = 78% (D−F), and sPP4 with [*rrrr*] = 70.6% (G−I), stretched at 60 °C at the indicated values of deformations ϵ. The $(020)_t$ and $(110)_t$ equatorial reflections and the $(021)_t$ and $(111)_t$ reflections on the first layer line of the trans-planar form III are indicated. On the first layer line reflections corresponding to the helical and trans-planar conformations are also indicated.

phic form probably corresponds to the equilibrium modification, thermodynamically stable at those values of stereoregularity and deformation.

The influence of temperature on the deformation behavior of s-PP has been investigated performing stretching of compression-molded films at temperatures of 6, 60, and 80 °C.

The X-ray fiber diffraction patterns of fibers of the samples sPP1 and sPP5, with [*rrrr*] = 91.5 and 60.1%, respectively, obtained by stretching at 6 °C at four values of strain, are reported in Figure 7 as an example. The profiles read along the equatorial line of the X-ray diffraction patterns of fibers of the samples sPP1 and sPP5 stretched at different deformations are reported in Figure 8. Also, at 6 °C the helical form I transforms into the trans-planar form III for the most syndiotactic sample sPP1 (Figure 7A−D) and into the mesomorphic form in the case of the less stereoregular sample sPP5 (Figure 7E−H).

It is apparent from Figures 7 and 8 that the values of critical strain ϵ_c at which the phase transition from the helical form I into the trans-planar form begins, upon stretching the samples at 6 °C, are similar to those found at room temperature, that is 90−100% for the highly stereoregular sample sPP1 (Figures 7B and 8A) and 100−150% for the less syndiotactic sample sPP5 (Figures 7F,G and 8B). On the other hand, the low stretching temperature stabilizes the helical form I and influences the values of minimum strain ϵ_{min} at which the transition is complete. For the most syndiotactic sample sPP1, indeed, the formation of the pure trans-planar form III is strongly delayed, due to the reduced mobility of the chains at low temperature, and occurs at $\epsilon_{min} \approx 600\%$ (Figures 7D and 8A), much higher

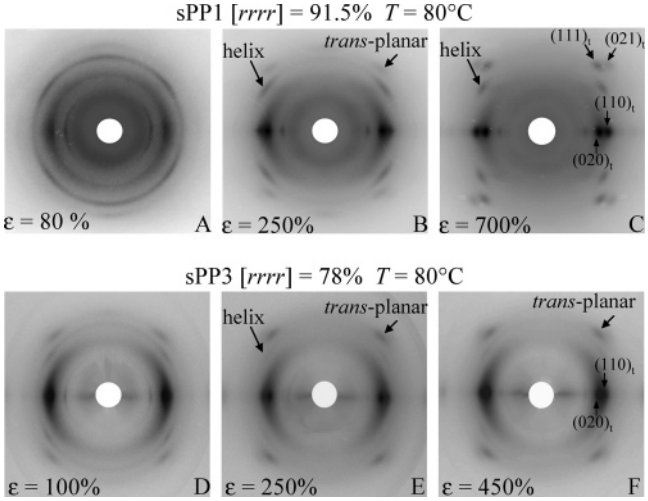

Figure 10. X-ray fiber diffraction patterns of fibers of the highly stereoregular samples sPP1 with [*rrrr*] = 91.5% (A−C) and sPP3 with [*rrrr*] = 78% (D−F), stretched at 80 °C at the indicated values of deformations ϵ. The $(020)_t$ and $(110)_t$ equatorial reflections and the corresponding $(021)_t$ and $(111)_t$ reflections on the first layer line of the trans-planar form III are indicated. On the first layer line reflections corresponding to the helical and trans-planar conformations are also indicated.

than that observed at room temperature (Figures 2 and 6). For the poorly syndiotactic sample sPP5, with [*rrrr*] = 60.1%, the pure trans-planar mesomorphic form does not form by stretching at 6 °C, even at very high deformations, and crystals in the helical form I persist in the fibers up to deformations close to the break, as indicated by the presence of the $(200)_h$ reflection in the patterns of Figures 7H and 8B.

The X-ray fiber diffraction patterns of fibers of the samples sPP1 ([*rrrr*] = 91.5%) and sPP3 ([*rrrr*] = 78%), stretched at 60 and 80 °C, and of the poorly syndiotactic sample sPP4 ([*rrrr*] = 70.6%), stretched at 60 °C, at three values of strain are reported in Figures 9 and 10. The profiles read along the equatorial line of the X-ray diffraction patterns of fibers of the samples sPP1 and sPP3, stretched at 60 and 80 °C, and of the sample sPP4, stretched at 60 °C, at different values of strain are shown in Figures 11 and 12.

From the data of Figures 7−12, the fractions of crystals of trans-planar forms ($f_{trans-planar}$) present in the fibers of the s-PP samples stretched at 6 and 60 °C have been evaluated using the procedure described above (Figure 4). The values of $f_{trans-planar}$ are reported in parts A and B of Figure 13 as a function of strain for the stretching temperatures of 6 and 60 °C, respectively. At high stretching temperatures a different behavior is observed depending on the stereoregularity.

In fact, for the most syndiotactic sample sPP1 with [*rrrr*] = 91.5% the values of the critical strain ϵ_c are poorly influenced by the stretching temperature and remain almost equal to those observed at room temperature. For instance, at the stretching temperatures of 60 and 80 °C the helical form I, initially present in the unstretched samples, starts transforming into the trans-planar form III already at ϵ = 80−100% (Figures 9A, 10A, 11A, and 12A).

For the less stereoregular samples sPP3 and sPP4, with [*rrrr*] = 78 and 70.6%, respectively, instead, the increase of the stretching temperature induces a decrease of the values of the critical strain ϵ_c at which the transition begins, with respect to those observed at room and lower temperatures. For instance, when the sample sPP3 is stretched at 60 and 80 °C, the structural transition of the helical form I into the trans-planar form starts at values of ϵ_c as low as 50% (Figures 9D and 11B), and the amount of trans-planar form is already very high at ϵ = 100% (Figures 9E, 10D, 11B, and 12B).

The differences of the critical values of strain between low and high temperatures amplify for the poorly syndiotactic samples. For instance, for the sample sPP4 with [*rrrr*] = 70.6%, a critical strain $\epsilon_c \approx 50\%$ has been found at the stretching temperature of 60 °C (Figures 9G and 11C), much smaller than that observed at room temperature (ϵ_c = 200%, Figure 6).

The data of Figures 9−12 and 13B clearly indicate that at high stretching temperatures the critical strain ϵ_c at which the polymorphic transition begins depends only slightly on the stereoregularity, at variance with the data at room and low stretching temperatures of Figures 2−8 and 13A, which show a stronger dependence of ϵ_c on the stereoregularity.

It is worth noting that the stretching at high temperatures produces an improvement of crystals of the trans-planar form III, as indicated by the sharpening of the $(020)_t$ and $(110)_t$ equatorial reflections at 2θ = 16° and 18° and the $(021)_t$ and $(111)_t$ reflections on the first layer line of form III in the fiber diffraction patterns of Figures 9C,F and 10C,F.

The stretching temperature also influences the stability of the polymorphic forms involved in the polymorphic transition. For all samples the value of minimum strain ϵ_m at which the transition of helical form into the trans-planar forms is complete increases with increasing the stretching temperature. In particular, when the stretching is performed at 60 °C, for the highly stereoregular samples sPP1 and sPP3 the helical form I persists in the fibers up to high values of deformation, and the pure trans-planar III is obtained only at 700−800% strain (Figures 9C,F and 11A,B). For less stereoregular samples the pure trans-planar mesomorphic form does not form, even at high values of strain close to the break, and fibers in mixtures of crystals of the helical form I and trans-planar mesomorphic form are obtained at the maximum possible deformation (Figures 9I and 11C). Also, in the case of the highly stereoregular samples sPP1 and sPP3, fibers in the pure trans-planar form III are never obtained at stretching temperature of 80 °C (Figures 10C,F and 12A,B). High stretching temperatures, indeed, stabilizes the helical form I and inhibits the transition into the trans-planar form III.[3b]

Moreover, while for samples with *rrrr* content lower than 90−87% the transition of the helical form I into the trans-planar form III by stretching at room and low temperatures involves the formation of the intermediate disordered mesomorphic form at moderate values of strain (Figures 2E−H and 3B), at high stretching temperatures the helical form I transforms directly into the trans-planar form III for samples with concentration of *rrrr* pentad up to nearly 80% (Figures 10D−F and 12B), and the mesomorphic form is observed only for lower syndiotactic samples with *rrrr* pentad content lower than 78% (Figures 9G−I and 11C).

The data of Figures 7−12 and the values of critical strains ϵ_c and ϵ_m at 6 and 60 °C derived from the plots of Figure 13 have allowed building the phase diagrams of s-PP at different temperatures, using the method described above. The phase diagrams at 6 and 60 °C are reported in parts A and B of Figure 14, respectively. The boundary lines between the regions of stability of the different polymorphic forms have been determined as described above for the phase diagram at room temperature.

It is apparent from Figures 6 and 14 that the values of critical strain associated with the beginning of the structural transitions at different temperatures show similar dependence on the stereoregularity of the polymer samples. In particular, the critical

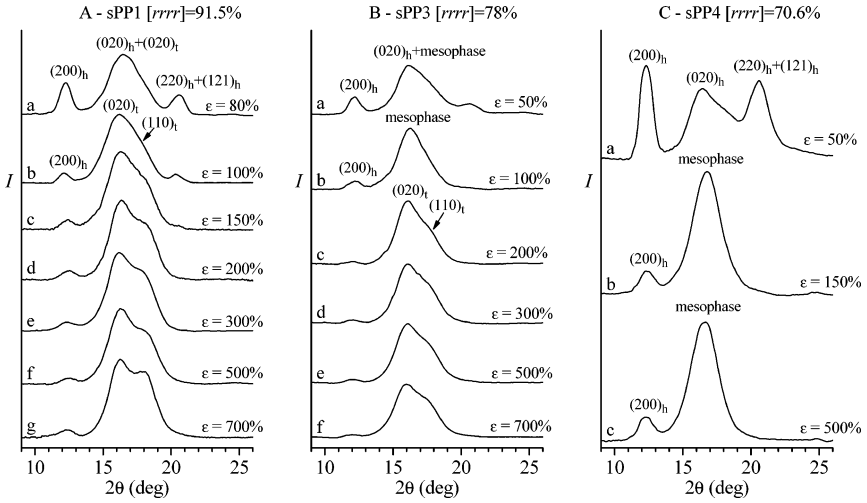

Figure 11. X-ray diffraction profiles read along the equatorial line, after the subtraction of the amorphous contribution, of the X-ray diffraction patterns of fibers of the samples sPP1 with [*rrrr*] = 91.5% (A), sPP3 with [*rrrr*] = 78% (B), and sPP4 with [*rrrr*] = 70.6% (C), stretched at 60 °C at the indicated values of deformation ϵ. The $(200)_h$, $(020)_h$, $(220)_h$, and $(121)_h$ reflections of the helical form I and the $(020)_t$ and $(110)_t$ reflections of the trans-planar form III are indicated.

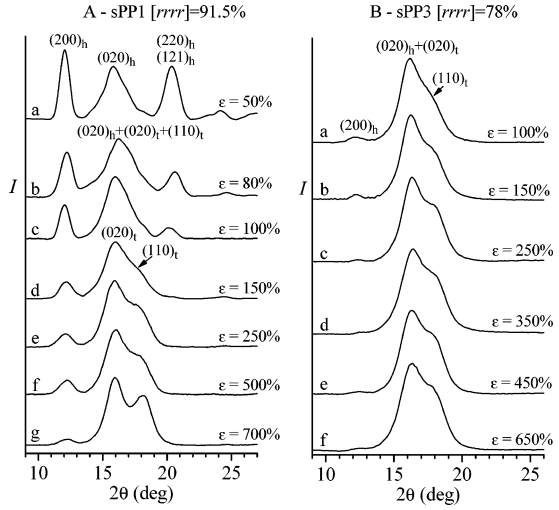

Figure 12. X-ray diffraction profiles read along the equatorial line, after the subtraction of the amorphous contribution, of the X-ray diffraction patterns of fibers of the samples sPP1 with [*rrrr*] = 91.5% (A) and sPP3 with [*rrrr*] = 78% (B), stretched at 80 °C at the indicated values of deformation ϵ. The $(200)_h$, $(020)_h$, $(220)_h$, and $(121)_h$ reflections of the helical form I and the $(020)_t$ and $(110)_t$ reflections of the trans-planar form III are indicated.

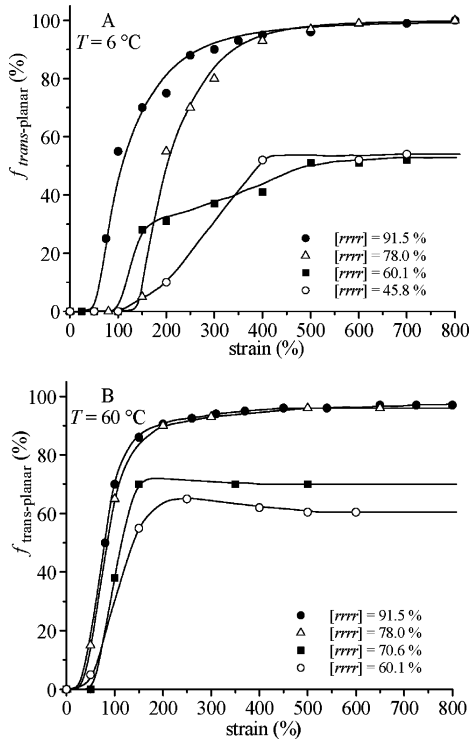

Figure 13. Fractions of crystals of trans-planar forms ($f_{trans-planar}$) present in the fibers of s-PP samples of different stereoregularity stretched at 6 °C (A) and 60 °C (B) as a function of strain.

strain increases with decreasing the concentration of *rrrr* pentad up to nearly 70% and then decreases for further decrease of stereoregularity (open circles in Figures 6 and 14A,B). This effect is reduced at high stretching temperature (Figure 14B). However, significant differences are observed in phase diagrams at different temperatures. First of all, the region of stability of the trans-planar form III is strongly reduced in the phase diagrams at 6 °C (Figure 14A) and 60 °C (Figure 14B) compared to that at room temperature (Figure 6). Moreover, the region of stability of the pure trans-planar mesomorphic form present in the phase diagram at room temperature for poorly stereoregular samples stretched at high deformations (Figure 6) disappears in the phase diagrams at 6 and 60 °C (Figure 14). Correspondingly, the regions of phase diagrams where mixtures of crystals of form I and form III, or form I and mesomorphic form, coexist are much larger at low and high temperatures (Figure 14) than at room temperature (Figure 6). This behavior reflects the reduced mobility at low stretching temperatures that delays the formation of the trans-planar form III and the trans-planar mesomorphic form for highly and poorly stereoregular s-PP samples, respectively, and the increased stability of the helical form I, compared to the trans-planar forms, at high stretching temperatures for all samples, regardless of stereoregularity.

Finally, the boundary line between the regions corresponding to (form I + form III) and (form I + mesophase) shifts toward lower values of *rrrr* pentad concentration with increasing stretching temperature (Figure 14B), so that the mesophase can be obtained at intermediate values of the strain at high stretching temperatures only for stereoirregular s-PP samples, with *rrrr* content lower than 78%. This is due to the annealing at high temperatures that favors the crystalline form III with respect to the mesomorphic form for highly stereoregular samples. The mesomorphic form is, therefore, obtained at high temperatures

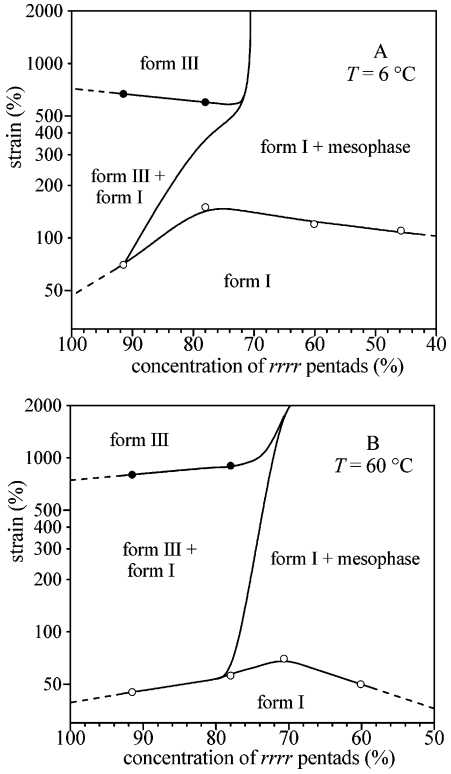

Figure 14. Phase diagrams of s-PP at 6 °C (A) and 60 °C (B) as a function of strain and stereoregularity.

only for low syndiotactic samples, where the formation of form III is prevented by the presence of high concentration of stereodefects.[6,13]

The data of Figure 6 and 14 have allowed building the phase diagrams of s-PP of a given stereoregularity as a function of strain and temperature. The phase diagrams for the samples sPP1, sPP3, and sPP5 with concentrations of *rrrr* pentad of 91.5, 78, and 60%, respectively, are reported in parts A, B, and C of Figure 15, respectively. In the case of the low syndiotactic sample sPP5 stretching procedures at temperatures higher than 60 °C were not performed due to softening of the sample at temperatures close to the melting temperature (T_m = 77 °C, see Table 1).

It is apparent that the conditions of formation of the trans-planar crystalline form III and mesomorphic form in stretched fibers of s-PP are basically linked to the stereoregularity. In fact, in highly stereoregular samples, with [*rrrr*] > 90%, the trans-planar mesomorphic form does not form by stretching at any deformation and temperature (Figure 15A). The helical form I initially present in the unstretched material transforms directly into the trans-planar crystalline form III when a critical value of stress, necessary for destruction of lamellar crystals, is achieved. The values of the critical strain linked to the polymorphic transitions are namely affected by the chain microstructure, whereas the corresponding values of the stress depend on the degree of crystallinity, the amount of structural disorder present in the crystals, and the relative stability of the two involved crystalline forms.

With decreasing stereoregularity, the phase diagram is complicated by the presence of a region of existence of the trans-planar mesophase, which forms in fibers stretched at moderate values of strain and at temperature below 60 °C (Figure 15B). In fact, at temperatures lower than 60 °C, when a critical value of stress is achieved, the mechanical melting of lamellae of the helical form I is followed by recrystallization of fibrils in the

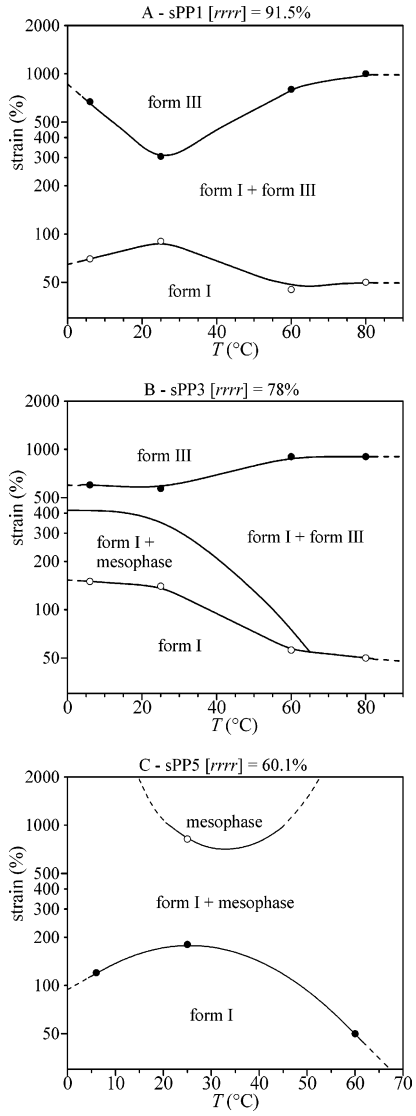

Figure 15. Phase diagrams of the samples sPP1 with [*rrrr*] = 91.5% (A), sPP3 with [*rrrr*] = 78% (B), and sPP5 with [*rrrr*] = 60.1% (C) as a function of strain and temperature. In (C) the boundary line between the regions corresponding to (form I + mesophase) and mesophase reflects the fact that at T > 50 °C the pure mesomorphic form could not be obtained even by stretching at strains close to the breaking of the sample specimen.

trans-planar mesomorphic form, which then transforms into the crystalline form III only at high values of strain (Figure 15B). For stretching temperatures higher than 60 °C the mesomorphic form does not form anymore, and probably, further crystallization of the amorphous phase also occurs during stretching. This produces a direct transition of the helical form I into the trans-planar crystalline form III already at low strains (Figure 15B), as occurs for highly stereoregular samples at any stretching temperatures (Figure 15A).

Finally, for poorly stereoregular samples, with [*rrrr*] lower than 70%, the trans-planar form III does not form at any deformation and stretching temperature (Figure 15C). The helical form I transforms, indeed, into the trans-planar mesomorphic form by stretching at any temperature. The pure mesomorphic form is obtained only by stretching at room temperature at high strains, whereas at lower and higher stretching temperatures only mixtures of helical form I and mesophase are obtained, even at high degrees of deformation (Figure 15C).

Concluding Remarks

The polymorphic behavior of s-PP in stretched fibers is rather complex, and the formation of different polymorphic forms by stretching depends on the stereoregularity, degree of deformation, and stretching temperature. A method for building the phase diagram of s-PP in stretched fibers as a function of stereoregularity, degree of deformation, and stretching temperature is reported. Determining the phase diagram of s-PP is of great interest because it allows for a correlation among stability of the different polymorphic forms, microstructural characteristics of the samples (the stereoregularity), and external parameters such as degree of deformation and temperature.

The different forms of s-PP in the phase diagrams are not considered from a thermodynamic standpoint but from the structure standpoint, based on the X-ray diffraction observations. The method is, indeed, based on the analysis of the X-ray fiber diffraction patterns of s-PP samples of different stereoregularity, prepared with different metallocene catalysts, stretched at different degrees of deformation and stretching temperatures. For all the analyzed samples the boundary lines between the different regions of stability of the different polymorphic forms have been determined by the emergence or disappearance of X-ray reflections typical of the different forms of s-PP, including the mesomorphic form.

Although the phase diagrams are given from a dynamic perspective rather than from a thermodynamic perspective, the used method guarantees that the critical values of strain, associated with the polymorphic transformations defining the boundary between different regions, are not affected by the deformation rate. In fact, the samples are kept in tension for 2 h during recording the X-ray fiber diffraction patterns, allowing full relaxation of the test specimen, and the observed polymorphic form probably corresponds to the equilibrium modification, thermodynamically stable at those values of stereoregularity and deformation.

The values of the critical strain at which the polymorphic transitions start and at which the transformation is complete depend on the stereoregularity. The extension of regions of stability of the helical form I, the trans-planar form III, and the mesomorphic form depends on the stretching temperature. The region of stability of the trans-planar form III is, indeed, much smaller at low and high temperatures than that at room temperature. Moreover, the region of stability of the pure trans-planar mesomorphic form present in the phase diagram at room temperature for poorly stereoregular samples stretched at high deformations disappears in the phase diagrams at low and high temperature.

Acknowledgment. Financial support from the "Ministero dell'Istruzione, dell'Università e della Ricerca" (PRIN 2004) is gratefully acknowledged. We thank Dr. Luigi Resconi of Basell Polyolefins (Ferrara, Italy) and Dr. Abbas Razavi of ATOFINA Research (Feluy, Belgium) for having provided the s-PP samples.

References and Notes

(1) (a) Loos, J.; Hückert, A.; Petermann, J. *Colloid Polym. Sci.* **1996**, *274*, 1006. (b) Loos, J.; Petermann, J.; Waldöfner, A. *Colloid Polym. Sci.* **1997**, *275*, 1088. (c) Loos, J.; Schimanski, T. *Polym. Eng. Sci.* **2000**, *40*, 567.

(2) (a) Schwarz, I.; Stranz, M.; Bonnet, M.; Petermann, J. *Colloid Polym. Sci.* **2001**, *279*, 506. (b) Bonnet, M.; Yan, S.; Petermann, J.; Zhang, B.; Yang, D. *J. Mater. Sci.* **2001**, *36*, 635.

(3) (a) Auriemma, F.; Ruiz de Ballesteros, O.; De Rosa, C. *Macromolecules* **2001**, *34*, 4485. (b) De Rosa, C.; Gargiulo, M.C.; Auriemma, F.; Ruiz de Ballesteros, O.; Razavi, A. *Macromolecules* **2002**, *35*, 9083. (c) De Rosa, C.; Ruiz de Ballesteros, O.; Auriemma, F. *Macromolecules* **2004**, *37*, 7724.

(4) Rodriguez-Arnold, J.; Zhang, A.; Cheng, S. Z. D.; Lovinger, A. J.; Hsieh, E. T.; Chu, P.; Johnson, T. W.; Honnell, K. G.; Geerts, R. G.; Palackal, S. J.; Hawley, G. R.; Welch, M. B. *Polymer* **1994**, *35*, 1884. Rodriguez-Arnold, J.; Bu, Z.; Cheng, S. Z. D.; Hsieh, E. T.; Johnson, T. W.; Geerts, R. G.; Palackal, S. J.; Hawley, G. R.; Welch, M. B. *Polymer* **1994**, *35*, 5194. Rodriguez-Arnold, J.; Bu, Z.; Cheng, S. Z. D. *J. Macromol. Sci., Rev. Macromol. Chem. Phys.* **1995**, *C35*, 117.

(5) (a) Auriemma, F.; De Rosa, C. *Macromolecules*, **2003**, *36*, 9396. (b) Auriemma, F.; De Rosa, C. *J. Am. Chem. Soc.* **2003**, *125*, 13143.

(6) (a) De Rosa, C.; Auriemma, F.; Ruiz de Ballesteros, O.; Resconi, L.; Fait, A.; Ciaccia, E.; Camurati, I. *J. Am. Chem. Soc.* **2003**, *125*, 10913. (b) De Rosa, C.; Auriemma, F.; Ruiz de Ballesteros, O. *Macromolecules* **2003**, *36*, 7607. (c) De Rosa, C.; Auriemma, F.; Ruiz de Ballesteros, O. *Macromolecules* **2004**, *37*, 1422.

(7) (a) Natta, G.; Corradini, P.; Ganis, P. *Makromol. Chem.* **1960**, *39*, 238. (b) Corradini, P.; Natta, G.; Ganis, P.; Temussi, P. A. *J. Polym. Sci., Part C* **1967**, *16*, 2477.

(8) Natta, G.; Peraldo, M.; Allegra, G. *Makromol. Chem.* **1964**, *75*, 215.

(9) (a) Lotz, B.; Lovinger, A. J.; Cais, R. E. *Macromolecules* **1988**, *21*, 2375. (b) Lovinger, A. J.; Lotz, B.; Davis, D. D. *Polymer* **1990**, *31*, 2253. (c) Lovinger, A. J.; Davis, D. D.; Lotz, B. *Macromolecules* **1991**, *24*, 552. (d) Lovinger, A. J.; Lotz, B.; Davis, D. D.; Padden, F. J. *Macromolecules* **1993**, *26*, 3494.

(10) De Rosa, C.; Corradini, P. *Macromolecules* **1993**, *26*, 5711.

(11) (a) Auriemma, F.; De Rosa, C.; Corradini, P. *Macromolecules* **1993**, *26*, 5719. (b) Auriemma, F.; De Rosa, C.; Corradini, P. *Rend. Fis. Accad. Lincei.* **1993**, *4*, 287.

(12) De Rosa, C.; Auriemma, F.; Vinti, V. *Macromolecules* **1997**, *30*, 4137.

(13) De Rosa, C.; Auriemma, F.; Vinti, V. *Macromolecules* **1998**, *31*, 7430.

(14) Rastogi, S.; La Camera, D.; van der Burgt, F.; Terry, A. E.; Cheng, S. Z. D. *Macromolecules* **2001**, *34*, 7730.

(15) Zhang, J.; Yang, D.; Thierry, A.; Wittmann, J. C.; Lotz, B. *Macromolecules* **2001**, *34*, 6261.

(16) Chatani, Y.; Maruyama, H.; Noguchi, K.; Asanuma, T.; Shiomura, T. *J. Polym. Sci., Part C* **1990**, *28*, 393.

(17) Chatani, Y.; Maruyama, H.; Asanuma, T.; Shiomura, T. *J. Polym. Sci., Polym. Phys.* **1991**, *29*, 1649.

(18) Auriemma, F.; De Rosa, C.; Ruiz de Ballesteros, O.; Vinti, V. *J. Polym. Sci., Part B: Polym. Phys.* **1998**, *36*, 395.

(19) (a) Nakaoki, T.; Ohira, Y.; Hayashi, H.; Horii, F. *Macromolecules* **1998**, *31*, 2705. (b) Ohira, Y.; Horii, F.; Nakaoki, T. *Macromolecules* **2000**, *33*, 1801. (c) Ohira, Y.; Horii, F.; Nakaoki, T. *Macromolecules* **2001**, *34*, 1655. (d) Ohira, Y.; Horii, F.; Nakaoki, T. *Macromolecules* **2000**, *33*, 5566.

(20) Vittoria, V.; Guadagno, L.; Comotti, A.; Simonutti, R.; Auriemma, F.; De Rosa, C. *Macromolecules* **2000**, *33*, 6200.

(21) (a) De Rosa, C.; Auriemma, F.; Ruiz de Ballesteros, O. *Polymer* **2001**, *42*, 9729. (b) De Rosa, C.; Ruiz de Ballesteros, O.; Santoro, M.; Auriemma, F. *Polymer* **2003**, *44*, 6267. (c) De Rosa, C.; Ruiz de Ballesteros, O.; Santoro, M.; Auriemma, F. *Macromolecules* **2004**, *37*, 1816.

(22) De Rosa, C.; Ruiz de Ballesteros, O.; Auriemma, F.; Savarese, R. *Macromolecules* **2005**, *38*, 4791.

(23) (a) Men, Y.; Strobl, G. *J. Macromol. Sci., Phys.* **2001**, *B40*, 775. (b) Men, Y.; Rieger, J.; Strobl, G. *Phys. Rev. Lett.* **2003**, *91*, 095502-1.

(24) (a) Hiss, R.; Hobeika, S.; Lynn, C.; Strobl, G. *Macromolecules* **1999**, *32*, 4390. (b) Hobeika, S.; Men, Y.; Strobl, G. *Macromolecules* **2000**, *33*, 1827.

(25) De Rosa, C.; Auriemma, F.; Ruiz de Ballesteros, O. *Phys. Rev. Lett.* **2006**, *96*, 167801.

(26) Ewen, J. A.; Jones, R.; Razavi, A.; Ferrara, J. D. *J. Am. Chem. Soc.* **1988**, *110*, 6255.

(27) Razavi, A.; Bellia, V.; De Brauwer, Y.; Hortmann, K.; Peters, L.; Sirole, S.; Van Belle, S.; Thewalt, U. *Macromol. Chem. Phys.* **2004**, *205*, 347.

(28) (a) Razavi, A.; Bellia, V.; De Brauwer, Y.; Hortmann, K.; Lambrecht, M.; Miserque, O.; Peters, L.; Van Belle, S. In *Metalorganic Catalysts for Synthesis and Polymerization*; Kaminsky, W., Ed.; Springer-Verlag: Berlin, 1999. (b) Razavi, A. Eur. Pat. Appl. 96111127,5. (c) Razavi, A. PCT/EP97/036449, Int. Appl. WO 98/02469, 1998, Atofina. (d) Haveaux, B.; Coupin, T. PCT/EP99/00371, Int. Appl. WO 99/37711, Atofina, 1999.

(29) (a) Razavi, A.; Thewalt, U. *J. Organomet. Chem.* **2001**, *621*, 267. (b) Razavi, A. PCT/EP00/08883, Int. Appl. WO 01/19877, Atofina, 2001.

(30) (a) Resconi, L.; Guidotti, S.; Baruzzi, G.; Grandini, C.; Nifant'ev, I. E.; Kashulin, I. A.; Ivchenko, P. V. PCT Int. Appl. WO 01/53360, Basell, Italy, 2001. (b) Grandini, C.; Camurati, I.; Guidotti, S.; Mascellari, N.; Resconi, L.; Nifant'ev, I. E.; Kashulin, I. A.; Ivchenko, P. V.; Mercandelli, P.; Sironi, A. *Organometallics* **2004**, *23*, 344.

(31) De Rosa, C.; Auriemma, F.; Di Capua, A.; Resconi, L.; Guidotti, S.; Camurati, I.; Nifant'ev, I. E.; Laishevtsev, I. P. *J. Am. Chem. Soc.* **2004**, *126*, 17040.

(32) De Rosa, C.; Auriemma, F.; De Lucia, G.; Resconi, L. *Polymer* **2005**, *46*, 9461.

MA061749I